Journal Name

ARTICLE

Supplementary Information

N-NO & NN-O bond cleavage dynamics in two- and three-body Coulomb explosion of the N2O2+ dication.

Krishnendu Gope, Itamar Luzon and Daniel Strasser*

Institute of Chemistry, Hebrew University of Jerusalem, Jerusalem, Israel

Received 00th January 20xx,
Accepted 00th January 20xx

DOI: 10.1039/x0xx00000x
www.rsc.org/

In the following we provide supplementary information Regarding the raw experimental data and its analysis procedure.

The blue bars in figure S1 show the measured yields of 20, 21 and 22 mass/charge ratios. Mass/charge 20 is assigned to the $^{20}Ne^+$ cation, which is introduced into the setup in the high order harmonic generation (HHG) region. Accordingly, the yellow bars show the expected yields of $^{21}Ne^+$ and $^{22}Ne^+$ isotopes estimated from their respective 90.48% :0.27% : 9.25% natural abundances.[1] Thus, we conclude that all the observed 21 and 22 mass/charge yields are assigned to the stable Ne isotopes and that the meta-stable N_2O^{2+} dication yield, also expected to appear at 22 mass/charge, is below our experimental detection limit. The statistical error limit is estimated to be ~ 0.1 Counts/ 10^6 laser shots, which is less than ~0.1% of the total dication Coulomb explosion yield detected as two cation coincidence events.

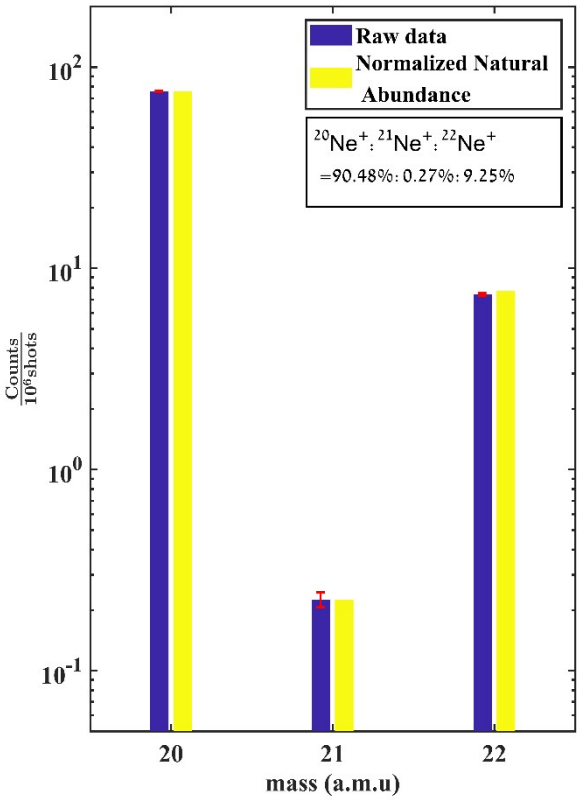

Figure S1: Comparation of $^{20}Ne^+$ $^{21}Ne^+$ and $^{22}Ne^+$ signals with their respective normalized natural abundances, showing that no significant N_2O^{2+} yield can be observed.

*strasser@huji.ac.il
†

KER Peak Position analysis

Figure S2a and S2b show the fitted KER peak positions for the NN-O and N-NO channels as a function of the near-IR time delay. The vertical error bars represent the fitting uncertainties corresponding to each KER peak position. Whereas the horizontal errorbars represent the time window in which the fitted KER spectrum was recorded. As described in the main text, the KER of both channels exhibit a shift towards lower KER as a function of time delay, reaching their asymptotic shift at ~700fs.

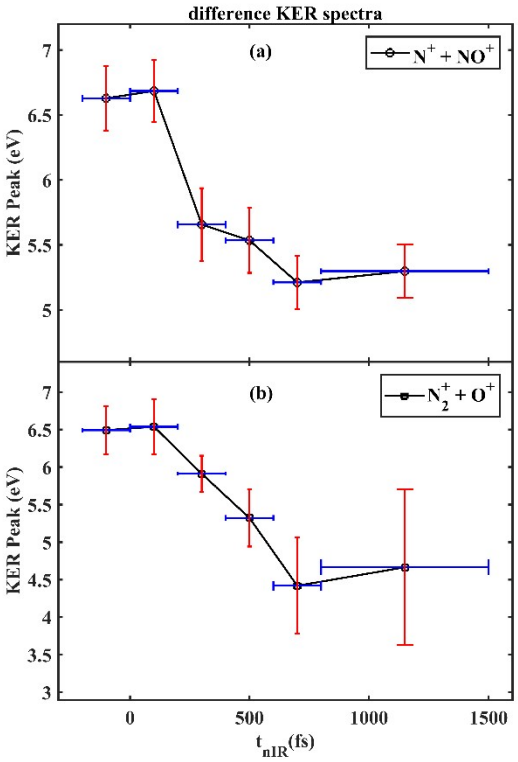

Figure S2: Showing the fitted KER peak position as a function of the near-IR time delay for (a) $N^+ + NO^+$ and (b) $N_2^+ + O^+$ channel. Here, the blue horizontal error bar indicates the time-delay window for which the KER spectrum is recorded.

Dalitz plot analysis

In order to show the relation between the raw measured data and the final Dalitz plots of the three-body break-up $A^+ + B^+ + C$ channels, we present the detailed stages of the data processing.

figure S3(a_1) shows the raw 2D Dalitz plot data of the $N^+ + N + O^+$ channel. As described in the main text, the mass weighted Dalitz plot η_1 and η_2 coordinates are constructed according to the following eq:

$$\eta_1 = \frac{15}{2\sqrt{44}} \times (\epsilon_{N1} - \epsilon_{N2})$$

$$\eta_2 = 2(\epsilon_O - 1)$$

Where $\epsilon_O, \epsilon_{N1}, and\ \epsilon_{N2}$ are the respective kinetic energy fractions carried away by the Oxygen and Nitrogen fragments, normalized by their maximal kinetic energy fraction allowed by energy and momentum conservation.

While N^+ and O^+ cation momenta are detected in coincidence, the neutral N momentum is evaluated based on total momentum conservation from the N^+ and O^+ center of mass recoil. As the center of mass resolution is superior in the 2D plane of the detector (due to VMI) [2], the raw Dalitz plots are obtained using only the 2D data.

The projection of 3D momentum correlation triangles on the 2D detector plane results in an artificial enhancement of the linear geometries.[3,4] This is illustrated in figure S3(b_1), showing a simulated 2D Dalitz plot of an uncorrelated uniform momentum correlation distribution, projected on a 2D plane.

In order to correct the artificial enhancement of linear geometries, figure S3(c_1) shows the weighted Dalitz plot (obtained by dividing figure S3(a_1) by figure S3(b_1).[3–5] Thus, the relative contributions of the different momentum correlation geometries exhibit their correct relative abundance.[3,4]

Figure S3(d_1) shows the random coincidence background from the measured dissociative ionization of two separate N_2O molecules. This distribution is directly derived from the measured raw data based on the absolute probability of uncorrelated events. As can be seen, the random coincidence background rate is negligible with respect to the true coincidence three body dissociation events. Nevertheless, figure S3(e_1) shows the background subtracted Dalitz plot, which is presented in figure 5(a) of the main manuscript.

Similarly, figures S3(a_2)- S3(e_2) show the analogous data analysis stages performed for the $N^+ + N^+ + O$ channel. Here, to allow critical evaluation of the raw data, figure S3(a_2) shows the raw data before the symmetrisation procedure due to the exchange of the two indistinguishable N^+ cations.

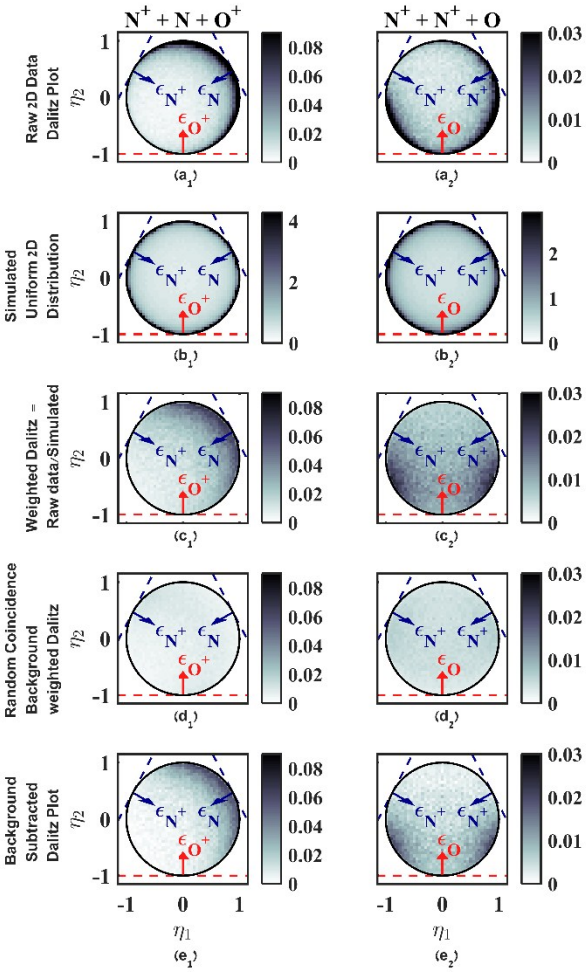

Figure S3: The detailed stages of the data processing for $N^+ + N + O^+$ and $N^+ + N^+ + O$ channels.

references

1 M. Berglund and M. E. Wieser, Isotopic compositions of the elements 2009 (IUPAC Technical Report), *Pure Appl. Chem.*, 2011, **83**, 397–410.

2 A. T. J. B. Eppink and D. H. Parker, Velocity map imaging of ions and electrons using electrostatic lenses: Application in photoelectron and photofragment ion imaging of molecular oxygen, *Rev. Sci. Instrum.*, 1997, **68**, 3477–3484.

3 D. Strasser, L. Lammich, H. Kreckel, S. Krohn, M. Lange, A. Naaman, D. Schwalm, A. Wolf and D. Zajfman, Breakup dynamics and the isotope effect in H_3^+ and D_3^+ dissociative recombination, *Phys. Rev. A - At. Mol. Opt. Phys.*, 2002, **66**, 327191–3271913.

4 D. Strasser, L. Lammich, H. Kreckel, M. Lange, S. Krohn, D. Schwalm, A. Wolf and D. Zajfman, Breakup dynamics and isotope effects in D_2H^+ and H_2D^+ dissociative recombination, *Phys. Rev. A*, 2004, **69**, 064702.

5 I. Luzon, E. Livshits, K. Gope, R. Baer and D. Strasser, Making Sense of Coulomb Explosion Imaging, *J. Phys. Chem. Lett.*, 2019, **10**, 1361–1367.